

Experimental Validation of a Novel Control Strategy for an Off-Grid Hybrid Stirling Engine/Supercapacitor Power Generation System

Mustapha Amine Rahmani* Mazen Alamir**
David Gualino* Sylvain Lechat Sanjuan*

* *Schneider Electric Industries, Grenoble, France (e-mail: mustapha.rahmani@schneider-electric.com, david.gualino@schneider-electric.com, sylvain.lechat-sanjuan@schneider-electric.com).*

** *University of Grenoble, Gipsa-lab, control Systems Department, France (e-mail: mazen.alamir@grenonle-inp.fr)*

Abstract: In this paper a novel optimal control strategy for energy management of an off-grid hybrid Stirling engine/Supercapacitor power plant is presented based on preliminary results proposed in [1]. An implementation of the control strategy is performed on a real time target that drives a dedicated testbed with a DC machine reproducing the behaviour of the thermodynamic Stirling Engine. The DC machine is linked to a Permanent Magnet Synchronous Generator (PMSG) connected to an AC load through an appropriate controlled Power electronics and an energy storage device which is a supercapacitor. The performances of the developed control Strategy are then assessed through experimental results on the testbed.

Keywords: Nonlinear Control; Power Electronics Control; Stirling Engine; Supercapacitor; Power Generation; Real time control implementation.

1. INTRODUCTION

Today, many populations throughout the developing countries suffer from the lack of electricity essentially because they are located in isolated villages where the electrical grid is not available or when it is, there is so much power demand (coming essentially from big cities) that it is highly disturbed. On the other side, the need for electricity of those populations is highly increasing. Nowadays, to supply those populations with electricity, traditional fuel based generators are used despite of their many drawbacks including their low reactivity to load changes, their high emissions and noise to mention but few issues.

In order to bring solutions to the energy access for those populations, Schneider Electric launched a program called BIP BOP¹ [2] that aims at bringing safe, clean and affordable electricity to populations that do not have access to it. Within the framework of this program, the MICROSOL project aims at developing micro solar thermodynamic plants producing a minimum of 150 kWh_{elec}/day functioning 24h/24 thanks to an appropriate thermal energy storage.

As a thermal to mechanical energy converter, the low temperature Stirling engine, working with the well known Stirling thermodynamic cycle [3], seems to be a promising solution because of its many advantages: simplicity of its

associated hydraulic circuit, robustness, low noise level, good thermal to electrical conversion efficiency to mention but few ones.

The aim of this paper is to present some experimental results that validate the control strategy that enables the adopted hybrid system to respond in real time to the varying load power demand in off-grid areas. The testbed dedicated to the validation of the proposed strategy is also presented.

In the literature, one can find many examples of hybrid power plants that use different renewable energy sources such as: wind, solar photovoltaic, hydraulic and fuel cells. Different control strategies either for grid or off-grid applications are also discussed. To respond in real time to load transients, an efficient control on the electrical part of the hybrid power plant is necessary. The control strategies go from PI-based controllers (see for example [4], [5]) to more sophisticated ones based for example on sliding mode techniques (see [6],[7],[8]). However most of these controllers don't necessarily induce optimal performance of the system in term of settling time which can lead to over-dimensioning of the buffer energy source especially when it consists of supercapacitors which is the case for our system because of their many advantages (see [9] for more details).

¹ For *Business, Innovation and People at the Base of the Pyramid*

This paper concerns the experimental validation on a dedicated testbed of the control strategy developed in [1] that stabilizes the studied hybrid power plant acting on the voltage conditioning stage.

This paper is organized as follows: section 2 describes the system under study. In section 3, the mathematical model of the system together with its state space equations are recalled based on [1]. In section 4, an analysis of the global system is performed and the control strategy developed in [1] recalled. In section 5 the experimental testbed is presented while in section 6 the performances of the developed control strategy are assessed through experimental results. Finally section 7 concludes the paper.

2. DESCRIPTION OF HYBRID POWER PLANT

The solar micro plant under study is depicted in Figure 1. It consists of a Stirling engine that generates mechanical work by performing a Stirling thermodynamic cycle at each shaft rotation. The produced motor torque together with the electromagnetic torque of the PMSG impose the rotational speed of the shaft. Due to the variable speed of the engine, the variable voltage amplitude and frequency at the output of the PMSG is conditioned through an appropriate power electronics to supply the AC load with a 230V 50Hz voltage. The voltage conditioning stage consists of a diode bridge linked to an isolated full bridge DC/DC converter connected to a DC bus whose voltage needs to be regulated at $V_{bus} = 50V$ which is the voltage compatible with the functioning of the AC/DC inverter that supply the AC load.

Because of the high mechanical and thermal inertia of the Stirling engine, an electrical energy buffer which is the supercapacitor is interfaced to the DC bus through a bidirectional DC/DC converter to absorb or deliver power during load transients in a fast manner while the Stirling engine adapts its delivered power on a rather medium time scale.

A second controller which is out of the scope of this paper, uses the informations on the temperatures of the hot and cold fluids at the inlet of the Stirling engine together with the power demand to compute the hot and cold mass flow rates leading to optimal net thermoelectric efficiency. In the work described in the present paper, the two mass flow rates of the hot and cold fluids are not used as control variables but are considered as constant. Only the control of the electrical stage is considered here. Obviously, the two parts show separable time scales so that the solutions proposed in this paper can be reused in a global architecture that manages to monitor the efficiency of the Stirling engine through the manipulation of these two flow rates.

3. MODELLING OF THE ENERGY CONVERSION SYSTEM

In a recent contribution [1], the mathematical model of the system described in Figure 1 was presented. This model is recalled here for convenience:

$$J_{rot} \cdot \frac{d\Omega(t)}{dt} = \alpha(\dot{m}_h, \dot{m}_c) \cdot \Omega(t) + \beta(T_h^{in}, T_c^{in}) - p \cdot \frac{3 \cdot \sqrt{3}}{\pi} \cdot \phi_f \cdot I_{red} - D_{fr} \cdot \Omega(t) \quad (1a)$$

$$\frac{dI_{red}}{dt} = -\frac{R_s}{L_s} \cdot I_{red} - \frac{3 \cdot p}{2 \cdot \pi} \cdot \Omega(t) \cdot I_{red} + \frac{3 \cdot \sqrt{3} \cdot p \cdot \phi_f}{2 \cdot \pi \cdot L_s} \cdot \Omega(t) - \frac{1}{2 \cdot L_s} \cdot V_{red} \quad (1b)$$

$$C_f \cdot \frac{dV_{red}}{dt} = I_{red} - k \cdot i_{Lfb} \cdot \alpha_{fb} \quad (1c)$$

$$L_{fb} \cdot \frac{di_{Lfb}}{dt} = k \cdot V_{red} \cdot \alpha_{fb} - V_{bus} \quad (1d)$$

$$C_{tot} \cdot \frac{dV_{bus}}{dt} = i_{Lfb} + i_{Lbb} - \frac{P_L}{\eta_{inv} \cdot V_{bus}} \quad (1e)$$

$$L_{bb} \cdot \frac{di_{Lbb}}{dt} = V_{sc} \cdot \alpha_{bb} - V_{bus} \quad (1f)$$

$$C_{sc} \cdot \frac{dV_{sc}}{dt} = -i_{Lbb} \cdot \alpha_{bb} \quad (1g)$$

Equation (1a) describes the rotor dynamics where $\Omega(t)$ is the shaft rotational speed, D_{fr} is the friction coefficient of the rotor, J_{rot} is the total inertia of the rotating parts. \dot{m}_h and \dot{m}_c are the mass flow rates of the hot and cold fluids at the inlet of the Stirling Engine, T_h^{in} and T_c^{in} are their respective temperatures. $\alpha(\cdot)$ and $\beta(\cdot)$ are functions that can be derived from experimental or knowledge based scenarios [10] and define the Stirling engine torque.

Equation (1b) gives the dynamics of the rectified current I_{red} in which R_s and L_s are the stator resistance and the stator self-inductance respectively, p is the number of pole pairs of the PMSG and ϕ_f the EMF constant of the motor. V_{red} is the rectified voltage whose dynamic is given by equation (1c) where C_f is the value of the output capacitor of the diode bridge.

Equation (1d) gives the dynamic of i_{Lfb} which is the output current of the DC/DC Full Bridge converter illustrated in figure 2 where α_{fb} is the duty ratio of the Full Bridge converter, L_{fb} is its output inductance and k is the transformer winding ratio.

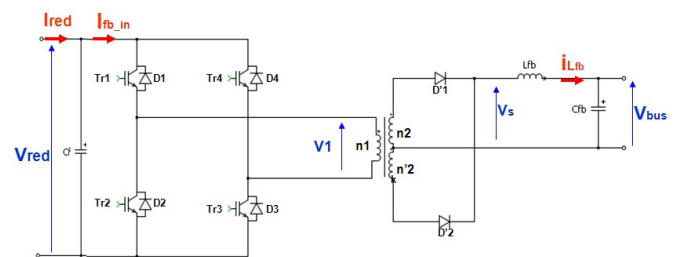


Fig. 2. DC/DC Full Bridge converter.

The duty ratio $\alpha_{fb} \in [0, 0.9]$ is one of the control signals of the developed feedback law. It is first conditioned before it is applied to drive the DC/DC Full Bridge converter as it is illustrated in Figure 3. In this figure, α_{fb} is first divided by two before generating its corresponding electrical signal α_{fb}^{elec} in order to drive the two pairs of Insulated Gate Bipolar Transistors (IGBT) (Tr_1, Tr_3) and (Tr_2, Tr_4), during a cutting frequency $T_{sw} = 20$ kHz, with the same period

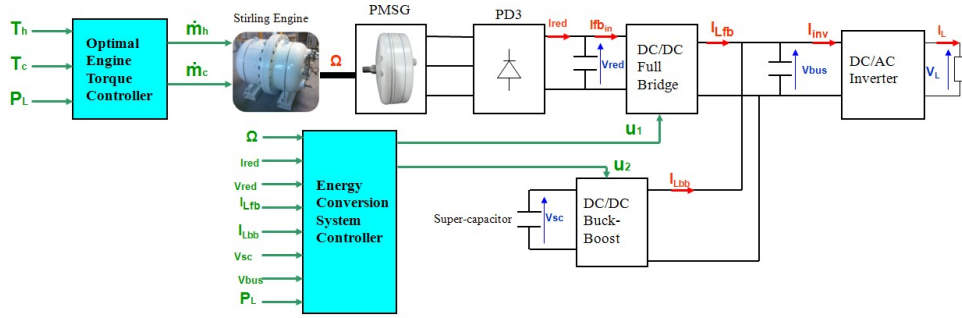


Fig. 1. Overview of the solar micro plant including the Stirling Engine and the PMSG together with its Power electronics.

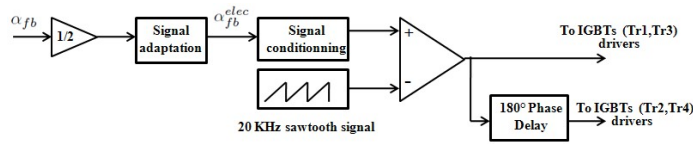


Fig. 3. DC/DC Full Bridge converter.

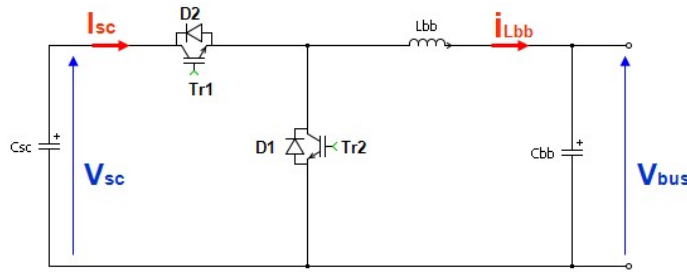


Fig. 4. Bidirectional DC/DC converter.

but 180° out of phase.

The DC bus equation is given by (1e) where C_{tot} is the total capacitance of the bus, P_L is the load power demand and η_{inv} is the electrical efficiency of the inverter. i_{Lbb} is the output inductance of the bidirectional DC/DC converter illustrated in figure 4 and whose equations are given by (1f)-(1g) where $\alpha_{bb} \in [0, 0.95]$ is the duty ratio of the bidirectional DC/DC converter, L_{bb} is the output inductance of this converter, C_{sc} is the supercapacitor capacitance and V_{sc} its voltage.

The equations of this bidirectional DC/DC converter were obtained considering a complementary control (see [11]) of this device which is generally preferred (because it avoids the discontinuous conduction mode of this converter), where, during a switching period, both IGBTs are used (but not simultaneously).

Despite the fact that the bidirectional DC/DC converter used in the testbed doesn't work in a complementary mode but during a switching period only one IGBT is activated at a time, the mean model (1f)-(1g) is still valid for control design with a slight modification before driving the converter. Indeed, the real duty ratio applied to the converter $\alpha_{bb}^{real} \in [-0.95, 0.95]$ is derived from α_{bb} as follow:

$$\alpha_{bb}^{real} = \alpha_{bb} - \frac{V_{bus}}{V_{sc}} \quad (2)$$

Finally, the duty ratio is transformed to a PWM signal using standard PWM techniques similar to the one of Figure 3 where Tr_1 (see Figure 4) is activated during a fraction of the switching period corresponding to $|\alpha_{bb}^{real}| \cdot T_{sw}$ if α_{bb}^{real} is positive otherwise Tr_2 will be activated during the same fraction of the switching period.

Gathering all the equations described so far leads to the following equations in the state space form:

$$\dot{x}_1 = a_1 \cdot x_1 - a_3 \cdot x_2 + a_2 \quad (3a)$$

$$\dot{x}_2 = -a_4 \cdot x_2 - a_5 \cdot x_1 \cdot x_2 + a_6 \cdot x_1 - a_7 \cdot x_3 \quad (3b)$$

$$\dot{x}_3 = a_8 \cdot x_2 - a_8 \cdot k \cdot x_4 \cdot u_1 \quad (3c)$$

$$\dot{x}_4 = -a_9 \cdot x_5 + k \cdot a_9 \cdot x_3 \cdot u_1 \quad (3d)$$

$$\dot{x}_5 = a_{10} \cdot (x_4 + x_6) - \frac{a_{10}}{\eta_{inv}} \cdot \frac{P_L}{x_5} \quad (3e)$$

$$\dot{x}_6 = -a_{11} \cdot x_5 + a_{11} \cdot x_7 \cdot u_2 \quad (3f)$$

$$\dot{x}_7 = -a_{12} \cdot x_6 \cdot u_2 \quad (3g)$$

where $x_1 = \Omega$, $x_2 = I_{red}$, $x_3 = V_{red}$, $x_4 = i_{Lfb}$, $x_5 = V_{bus}$, $x_6 = i_{Lbb}$, $x_7 = V_{sc}$. The control variables are: $u_1 = \alpha_{fb}$ and $u_2 = \alpha_{bb}$ corresponding to both duty ratios of the DC/DC Full Bridge and bidirectional DC/DC converter respectively. The coefficients a_i used in the state equations are given by: $a_1 = \frac{\alpha(\dot{m}_h, \dot{m}_c) - D_{fr}}{J_{rot}}$, $a_2 = \frac{\beta(T_{H_{in}}, T_{C_{in}})}{J_{rot}}$, $a_3 = \frac{p \cdot 3 \cdot \sqrt{3} \cdot \Phi_f}{\pi \cdot J_{rot}}$, $a_4 = \frac{R_s}{L_s}$, $a_5 = \frac{3 \cdot p}{2 \cdot \pi}$, $a_6 = \frac{p \cdot 3 \cdot \sqrt{3} \cdot \Phi_f}{2 \cdot \pi \cdot L_s}$, $a_7 = \frac{1}{2 \cdot L_s}$, $a_8 = \frac{1}{C_f}$, $a_9 = \frac{1}{L_{fb}}$, $a_{10} = \frac{1}{C_{tot}}$, $a_{11} = \frac{1}{L_{bb}}$, $a_{12} = \frac{1}{C_{sc}}$.

4. SYSTEM ANALYSIS AND CONTROLLER DESIGN

4.1 Control objectives and system constraints

In order to get a stable power electronics associated to the thermodynamic motor (which is reproduced on the testbed by a DC machine), two principal control objectives have to be reached:

- regulate $x_5 = V_{bus}$ around $x_5^{st} = V_{bus}^{ref} = 50V$ which is compatible with the good functioning of the commercial inverter.
- maintain $x_7 = V_{sc}$ around $x_7^{st} = V_{sc}^{ref} = 110V$ to always have an adequate amount of energy in the supercapacitor.

This system is also subject to the following constraints:
✓ positivity constraints $x_i \geq 0$ except $x_6 = i_{Lbb}$ since the bidirectional DC/DC converter is a current reversible

converter.

✓ strong saturations on control variables since:

- $u_1 \in [0, 0.9]$: duty ratio of the DC/DC Full Bridge.
- $u_2 \in [0, 0.95]$: duty ratio of the bidirectional DC/DC converter.

4.2 Global analysis of the system

By computing the values of the parameters a_i involved in the state equations (3) and given in section 5, it appears that the term " $a_5.x_1.x_2$ " corresponding to the output voltage drop of the diode bridge can be neglected compared to the other terms in equation (3b). Analysing the structure of the state space model given by equations (3), one can see that it is possible to split the system into two subsystems:

1) **The first subsystem** given by (3a)-(3d) and involves only u_1 as a control variable. This subsystem depends also on x_5 , but assuming that this variable is perfectly regulated around its reference (this will be proved later), x_5 can be replaced by its stationary (desired) value x_5^{st} . Therefore, subsystem (3a)-(3d) can be rewritten in the following condensed form:

$$\dot{z} = A(u_1).z + B. \begin{pmatrix} a_2 \\ x_5^{st} \end{pmatrix} \quad (4)$$

where $z = (x_1 \ x_2 \ x_3 \ x_4)^T$ is a reduced state vector.

2) **The second subsystem** corresponding to equations (3e)-(3g) where u_2 is the only control variable being involved.

In the next subsections, equations of subsystem 2 are used to regulate $x_5 = V_{bus}$ at $x_5^{st} = V_{bus}^{ref} = 50V$ in a fast manner using the control variable u_2 and to define an appropriate reference value for $x_4 = i_{Lfb}$ namely x_4^{st} that will adapt the state of charge of the supercapacitor by maintaining $x_7 = V_{sc}$ around $x_7^{st} = V_{sc}^{ref} = 110V$. Given x_4^{st} , a stationary value for u_1 namely u_1^{st} and its corresponding stationary value for z namely $z^{st}(u_1^{st})$ are derived and using the equations of subsystem 1, $z^{st}(u_1^{st})$ will be tracked by an appropriate control strategy acting on the control variable u_1 on a rather slower manner compared to subsystem 2 (this is due to the slow mechanical dynamic associated to the Stirling engine and the motor shaft). This is shown more precisely in the following sections. Note that since the two subsystems evolve in separate time scales, the decoupling of the global system is therefore justified.

4.3 Analysis and control of subsystem 1

Examination of the eigenvalues of $A(u_1)$ for a given constant $u_1 \in [0, 0.9]$ shows that the subsystem 1 is open-loop stable with highly oscillatory modes resulting in oscillatory open-loop state trajectories that would almost systematically lead to positiveness constraints violation. The control law used to stabilize z at some z^{st} (defined by u_1^{st} as it is shown later in section 4.4) is a one step² predictive control [12], namely:

$$u_1^{opt} = \arg \min_{u_1 \in [0, 0.9]} J(u_1) := \left\| z^+(u_1) - z^{st} \right\|_{P_d(u_1^{st})}^2 \quad (5)$$

² because of the limitation on the sampling time that is fixed to 100 μs .

where $z^+(u_1)$ given by (6) is the predicted value of the state vector z at the next time step based on the second order approximation of the exponential term. $P_d(u_1^{st})$ is the Lyapunov stability matrix of subsystem 1 (depending on u_1^{st}). Recall that the optimal problem (5) is defined for a given u_1^{st} which is defined once x_4^{st} is known (See section 4.4). The way x_4^{st} is defined is explained in the sequel. In order to solve (5) during the short sampling period, the differential equation (4) is approximated by a second order approximation namely:

$$z^+(u_1) = A_d(u_1)z + B_d(u_1). \begin{pmatrix} a_2 \\ x_5^{st} \end{pmatrix} \quad (6)$$

The resulting scalar optimal problem can then be solved by standard SQP (Sequential Quadratic Programming) iterations.

Note that while implementing the algorithm corresponding to equation (5), it has been considered only one weighting matrix $P_d(0.45)$ corresponding to a central value of $u_1^{st} = 0.45$. This has led to very good experimental results as it is shown in section 6.

4.4 Deriving u_1^{st} and z^{st} knowing x_4^{st}

Knowing x_4^{st} (see section 4.5), one can online compute the components of the desired values of the state vector z namely z^{st} and u_1^{st} by solving the set of the four equations corresponding to $\dot{z} = 0$. This leads to:

$$x_2^{st} = \frac{-B + \sqrt{\Delta}}{2.A}, \quad x_1^{st} = \frac{a_3.x_2^{st}}{a_1}, \quad x_3^{st} = \frac{x_4^{st}.x_2^{st}}{x_2^{st}}, \quad u_1^{st} = \frac{x_2^{st}}{k.x_4^{st}}$$

where: $A = \frac{a_3.a_6}{a_1} - a_4$, $B = \frac{-a_2.a_6}{a_1}$, $C = -a_7.x_4^{st}.x_5^{st}$ and $\Delta = B^2 - 4.A.C$.

4.5 analysis and control of subsystem 2

Since the equations (3e)-(3f) are in the strict-feedback form, a backstepping controller [13] is used to stabilize $x_5 = V_{bus}$ around $x_5^{st} = V_{bus}^{ref} = 50V$ leading to the following feedback law for u_2 :

$$u_2 = \frac{1}{a_{11}.x_7}. (a_{11}.x_5 - a_{10}.(x_5 - x_5^{st}) + \dot{x}_6^{ref} - \lambda_6.(x_6 - x_6^{ref})) \quad (7)$$

where

$$x_6^{ref} = \frac{P_L}{\eta_{inv} \cdot x_5} - x_4 + \frac{\lambda_5}{a_{10}}(x_5^{st} - x_5) \quad (8)$$

λ_5 and λ_6 are the design parameters of the backstepping controller.

According to simulations performed in [1], it was proved that the previous backstepping approach leads to a stiff controller in u_2 that rapidly stabilizes x_5 around x_5^{st} leading to ($\dot{x}_5 \approx 0$):

$$x_6 = -x_4 + \frac{P_L}{\eta_{inv}.x_5^{st}} \quad (9)$$

Then, by setting the following appropriate stationary reference value for x_4 (that will be tracked by subsystem 1 using u_1 as it was explained in previous sections) namely:

$$x_4^{st} = -k_6. \tanh(\beta.(x_7 - x_7^{st})) + \frac{P_L}{\eta_{inv}.x_5^{st}} \quad (10)$$

this would lead to the following stationary value for x_6 :

$$x_6^{st} = k_6. \tanh(\beta.(x_7 - x_7^{st}))$$

which together with equation (3g) stabilizes x_7 around x_7^{st} .

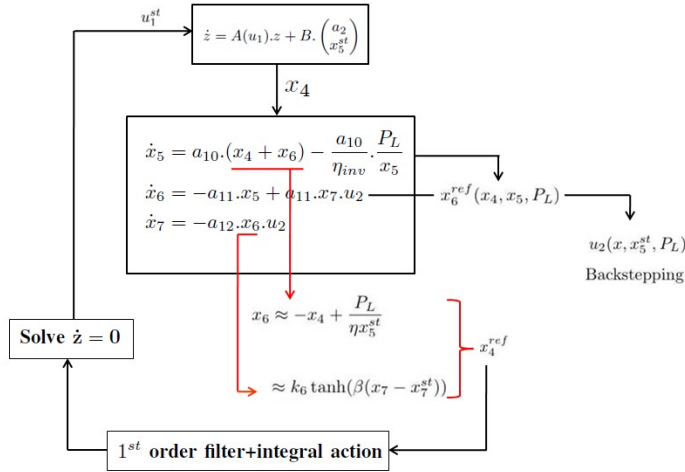


Fig. 5. Global control architecture for the complete system.

As it was observed from simulations performed in [1], x_4 undergoes an undershoot (or an overshoot) during positive (or negative) step changes in x_4^{st} , which can lead to constraints violation. To solve this problem, the reference value x_4^{st} given by equation 10 is filtered to smooth the convergence of x_4 and a corrective term (slow integrator) is added to x_4^{st} (before the filtering) to correct the static error on x_4 (which is a crucial state variable that adapts the state of charge of the supercapacitor) due to some model uncertainties. This leads to the following modified reference value for x_4 namely x_4^* in the discrete form:

$$x_4^*(k+1) = \alpha_f \cdot (x_4^{st}(k) + \epsilon(k)) + (1 - \alpha_f) \cdot x_4^*(k) \quad (11a)$$

$$\epsilon(k+1) = k_{aw} \cdot \epsilon(k) + \eta_{corr} \cdot (x_4^{st}(k) - x_4(k)) \quad (11b)$$

where α_f is a filtering parameter, η_{corr} is the integrator gain and k_{aw} is an anti windup gain.

Figure 5 summarises the global control scheme that leads to a stable and efficient voltage conditioning stage associated to the Stirling Engine.

5. DESCRIPTION OF THE EXPERIMENTAL TESTBED

Before testing the developed control on the real thermodynamic Stirling engine, an experimental testbed was built aiming at validating and assessing the performances of the feedback laws. On this testbed, a DC machine reproduces the behaviour of the Stirling engine by controlling the DC machine torque using a commercial DC drive. The DC machine is then linked to the PMSG connected to the developed power electronics as it is shown in Figure 6. A programmable AC load connected at the output of the single phase inverter is used to generate variable load profiles.

The developed control strategy is then transcribed in MATLAB/Simulink[®] environment and ".dll" file embedding a C code is generated thanks to Simulink coder[®]. The generated file is then deployed on a National Instrument real time target using the National Instrument Veristand[®] platform (installed on a host PC) that is also

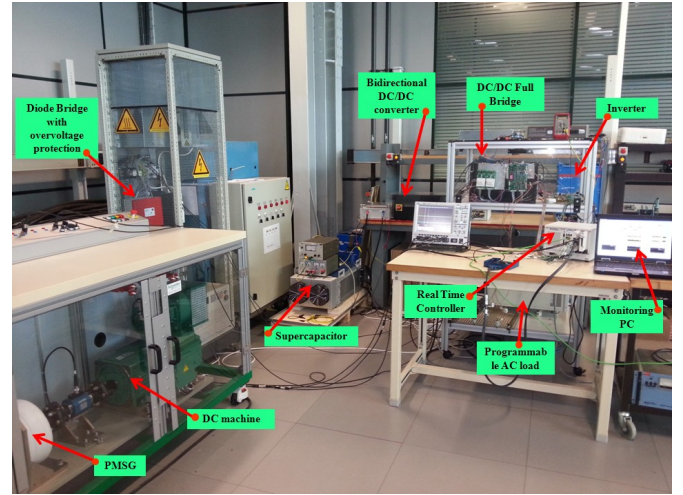


Fig. 7. Testbed used for experimental validation and performance assessment of the proposed control strategy.

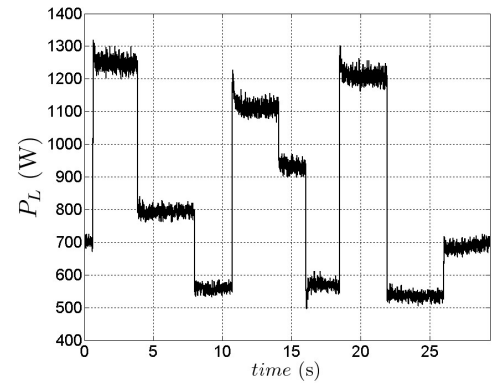


Fig. 8. Load power demand P_L at the input of the inverter.

used to monitor and make data acquisitions.

An overview of the experimental testbed is depicted in Figure 7. The system parameters that hold for the experimental testbed are given by:

PMSG nominal power: 1.8 kW, $J_{rot}=0.0672 \text{ Kg.m}^2$, $\alpha(\dot{m}_h, \dot{m}_c)=-0.0111$, $\beta(T_{H_{in}}, T_{C_{in}})=45$, $\phi_f=0.6014$, $R_s=5$, $L_s=0.28 \text{ m.H}$, $p=8$, $C_f=2400 \mu.F$, $L_{fb}=150 \mu.H$, $L_{bb}=223 \mu.H$, $C_{fb}=50 \mu.F$, $C_{bb}=136 \text{ m.F}$, $C_{SC}=63 \text{ F}$.

This leads to the following numerical values for a_i parameters: $a_1 = -0.183$, $a_2 = 558.11$, $a_3 = 118.4453$, $a_4 = 9615.4$, $a_5 = 1.3712$, $a_6 = 5101.1$, $a_7 = 641.02$, $a_8 = 425.53$, $a_9 = 6666.7$, $a_{10} = 7.34$, $a_{11} = 4484.3$, $a_{12} = 0.0159$, $\eta_{inv} = 0.95$ and $k = 0.5$.

6. EXPERIMENTAL RESULTS

In this section, some experimental results that validate and assess the performances of the proposed control strategy are presented and discussed. Through the programmable AC load (connected to the output of the inverter) depicted in Figure 6, a load power demand profile is generated and depicted in Figure 8 where the power is measured at the input of the inverter.

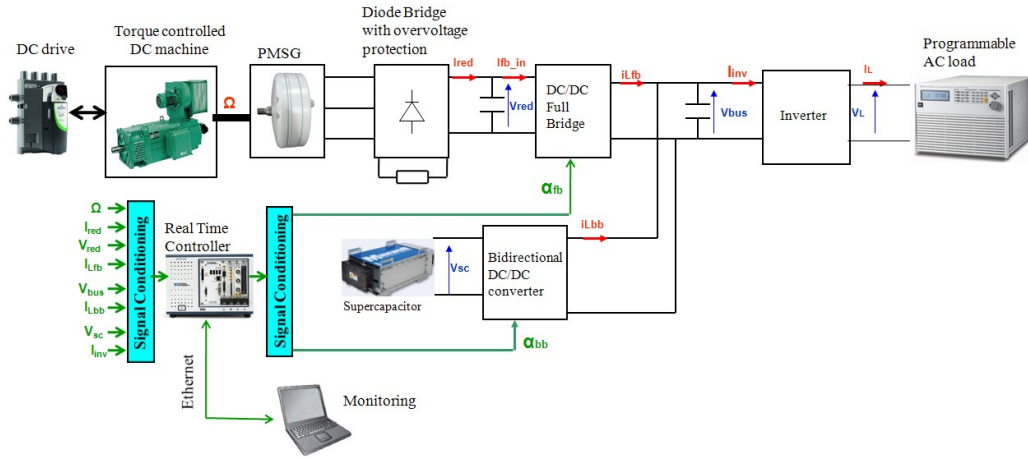


Fig. 6. Overview of the testbed together with its Power electronics.

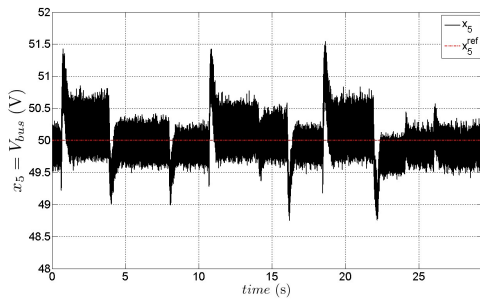


Fig. 9. Bus voltage V_{bus} and its reference value V_{bus}^{ref} .

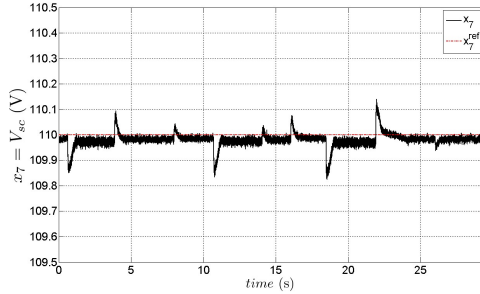


Fig. 10. Supercapacitor voltage V_{sc} and its reference value V_{sc}^{ref} .

Figure 9 shows that despite the sharp changes in the load power demand, the DC bus is perfectly regulated around its reference value of 50V which guarantees the good functioning of the inverter that supplies the AC load with uninterrupted 230V 50Hz voltage.

In Figure 10, one can see that the controller maintains the supercapacitor voltage at its desired reference value of 110V after each step in the power demand in order to always have enough energy (and free energy stock) to supply (or absorb) during future increase (or decrease) in the load power demand.

As discussed in previous sections, in order to accommodate dynamically for the load demand and maintain the supercapacitor voltage to its setpoint, a reference value for the output current of the DC/DC Full Bridge converter namely x_4^{st} is generated and depicted in Figure 12. This

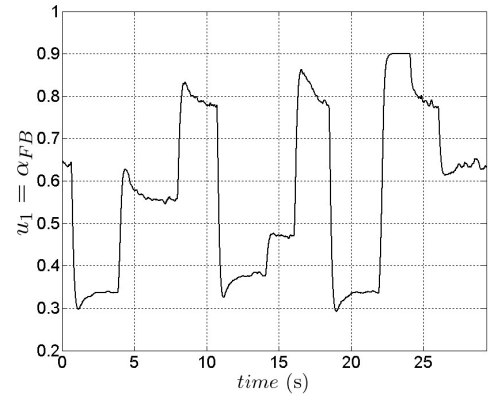


Fig. 11. Duty ratio of the DC/DC Full Bridge converter.

reference value is then used to generate, according to section 4.4, the reference values $x_1^{ref} = \Omega^{ref}$, $x_2^{ref} = I_{red}^{ref}$ and $x_3^{ref} = V_{red}^{ref}$ depicted in Figure 13. Then, the controller uses the duty ratio signal for the DC/DC Full Bridge converter namely $u_1 = \alpha_{fb}$ depicted in Figure 11 to track these references. As seen in Figure 12, the current i_{Lfb} is tracked with good response time allowing to rapidly adapt the state of charge of the supercapacitor. Figure 13 shows that the rotational speed, the rectified voltage and the rectified current also follow their respective reference despite the small static error coming from the modification of the reference signal for x_4 according to (11). However this static error will not affect the global dynamic of the system since the crucial objective being the regulation of $x_4 = i_{Lfb}$.

7. CONCLUSION

In this paper, an experimental validation on a dedicated testbed of a control strategy for the energy management of a hybrid Stirling engine/Supercapacitor power generation system has been presented. The experimental results show good performances for the proposed control architecture in responding in real time to load power demand transients while keeping the state of charge of the supercapacitor at an appropriate level. Future work will deal with incorporating the proposed controller within a global control scheme involving optimal torque control of the Stirling

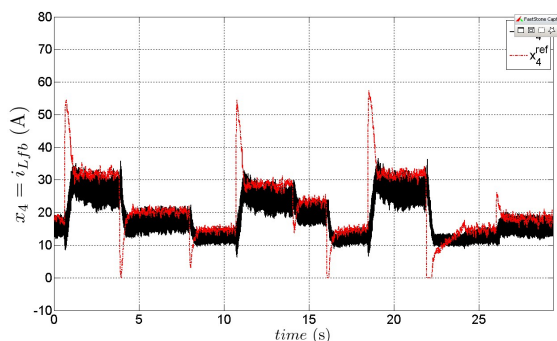


Fig. 12. Output current of the DC/DC Full Bridge converter i_{Lfb} and its reference value i_{Lfb}^{ref} .

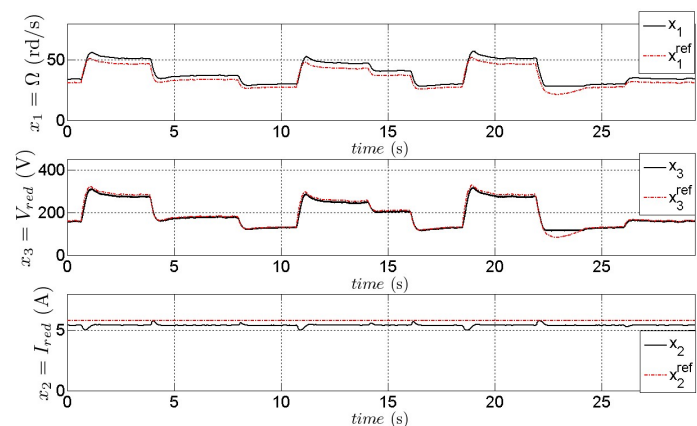


Fig. 13. Rotational speed of the engine Ω , the rectified voltage V_{red} and the rectified current I_{red} with their respective reference values Ω^{ref} , V_{red}^{ref} and I_{red}^{ref} .

engine and test the global controller on a testbed including the real thermodynamic Stirling engine also available within Schneider Electric.

REFERENCES

- [1] M. A. Rahmani, M. Alamir and D. Gualino *Control Strategy for an off-grid Stirling engine/supercapacitor power generation system*. Proceedings of the American Control Conference, Washington DC. USA, 2013.
- [2] Schneider Electric website: <http://www.schneider-electric.com/sites/corporate/en/group/sustainable-development-and-foundation/social-commitments/communities.page>
- [3] Mechanical department of Ohio University website: <http://www.ohio.edu/mechanical/stirling/me422.html>
- [4] N. Mendis, K.M. Muttaqui, S. Perera, and M.N. Uddin, A Novel Control Strategy for Stand-alone Operation of a Wind Dominated RAPS System, Industry Applications Society Annual Meeting (IAS), pp. 1-8, 2011.
- [5] N.A. Ahmed, A.K. Al-Othman, and M.R. Alrashidi, Development of an efficient utility interactive combined wind/photovoltaic/fuel cell power system with MPPT and DC bus voltage regulation, Electric Power Systems Research, vol. 81, pp. 1096-1106, 2011.
- [6] F. Valenciaga, P.F. Puleston, P.E. Battaiotto, and R.J. Mantz, Passivity/sliding mode control of a stand-alone hybrid generation system, IEE Proc.-

Control Theory Appl., vol. 147,NO. 6, pp. 680-686, 2000.

- [7] F. Valenciaga, P.F. Puleston, and P.E. Battaiotto, Variable structure system control design method based on a differential geometric approach: application to a wind energy conversion subsystem, IEE Proc.-Control Theory Appl., vol. 151,NO. 1, pp. 6-12, 2004.
- [8] F. Valenciaga, and P.F. Puleston, High-Order Sliding Control for a Wind Energy Conversion System Based on a Permanent Magnet Synchronous Generator, IEEE transactions on energy conversion, vol. 23,NO. 3, pp. 860-867, 2008.
- [9] O. Langlois, Conception d'un reseau de secours electrique pour l'aeronautique, Ph.D. dissertation, Dept. Genie Electrique, Institut National Polytechnique de Toulouse, Toulouse, 2006.
- [10] D.Meyer, Modelisation et controle commande d'un moteur Stirling pour une Micro Centrale Solaire Thermodynamique (MicST), master thesis dissertation, Dept. Automatique, Institut National Polytechnique de Grenoble, Grenoble, 2011.
- [11] T.L. Skvarenina, The power electronics handbook. Indiana: Purdue University, 2002.
- [12] D.Q. Mayne, J.B. Rawlings, C.V. Rao and P.O. Scokaert, Constrained model predictive control: stability and optimality, Automatica, vol. 36, pp. 789-814, 2000.
- [13] H.K. Khalil, NON LINEAR SYSTEMS, 2nd ed., Ed. Michigan: Prentice Hall, 1996, pp. 588-601.